Science Advances
AAAS

Supplementary Materials for

Single-molecule tracking reveals dynamic regulation of ribosomal scanning

Hea Jin Hong *et al.*

Corresponding author: Seán E. O'Leary, sean.oleary@ucr.edu

Sci. Adv. **10**, eadm9801 (2024)
DOI: 10.1126/sciadv.adm9801

The PDF file includes:

Other Supplementary Material for this manuscript includes the following:

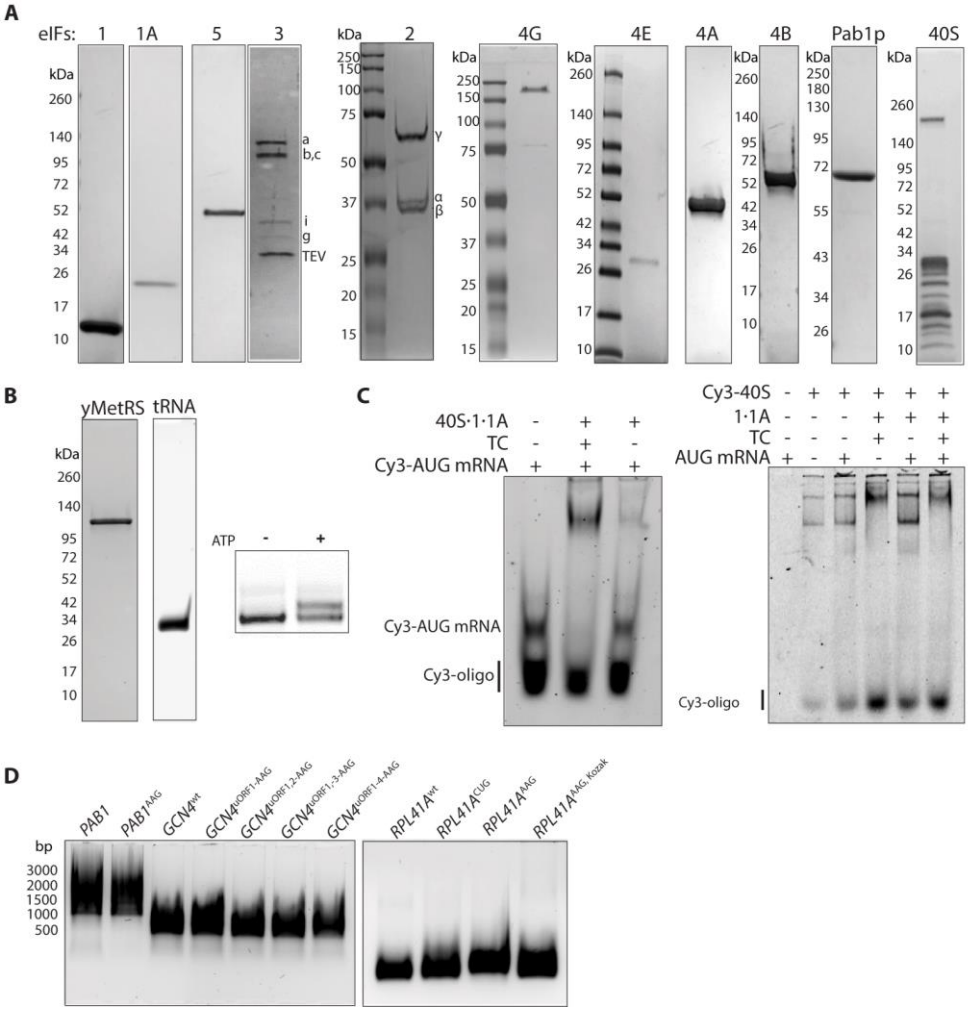

Fig. S1. Purification and validation of reagents. (A) SDS-PAGE analysis of purified individual components of the yeast PIC. **(B)** SDS-PAGE analysis of yeast methionyl transferase (yMetRS) and urea-PAGE analysis of *in vitro* transcribed tRNA. Acid-gel analysis of methionylation efficiency (right) **(C)** EMSA of the reconstituted PIC containing Cy3-model (*AUG*) mRNA, eIF1, eIF1A, and the eIF2 ternary complex formed with GDPNP (left). The gel on the right represents PIC formation with the Cy3-labelled 40S subunit. **(D)** *In vitro* transcribed RNAs on a TBE agarose gel.

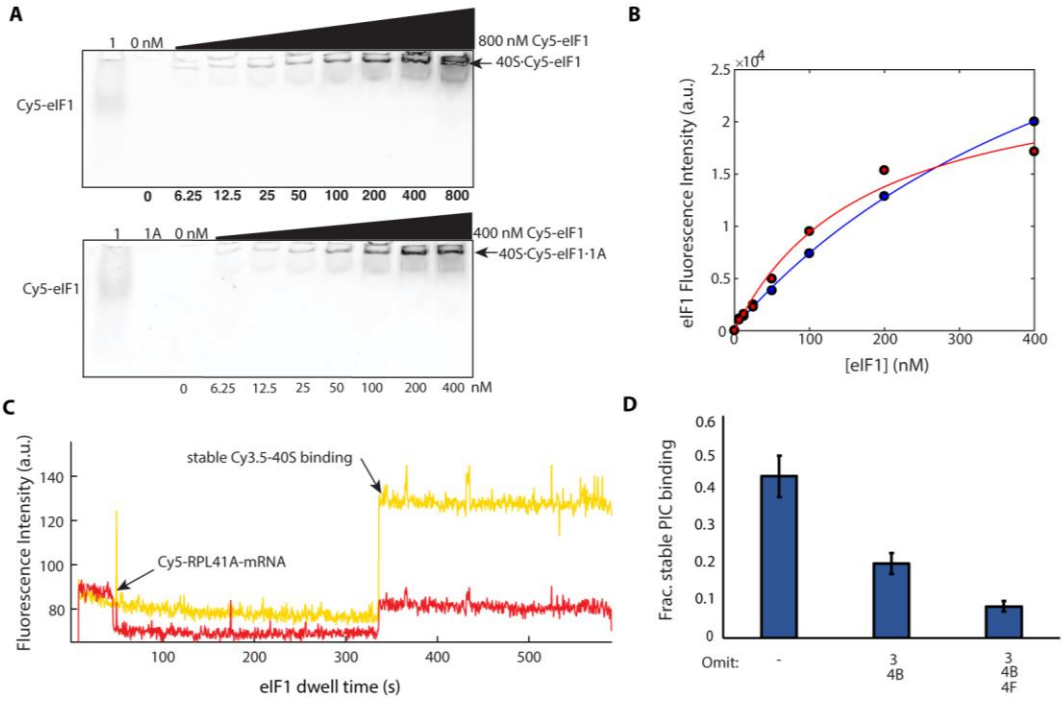

Fig. S2. Validation of PIC assembly and on-pathway PIC–mRNA loading. (A) Gel shift assay of Cy5-labelled eIF1 titrated against 40S subunits in absence and presence of eIF1a. **(B)** 40S-associated eIF1 band intensities were fit to the Langmuir isotherm (K_D = 575.7 without eIF1A (blue), and K_D= 175.7 with eIF1A (red)) **(C)** Idealized single-molecule fluorescence trace for Cy5-labelled *RPL41A* mRNA with Cy3.5-40S stably binding to the RNA. The experiment contains eIFs 1, 1A, 3, 5, 4A, 4G, 4B, eIF2 ternary complex, along with ATP and GTP. **(D)** Fraction of stable PIC binding under the assay conditions from panel C, modified by omission of the indicated factor(s). Error bars represent the standard deviation from 10,000 bootstrap samples of four randomly chosen sets of molecules within each condition (n = 148, 144, 123, 142 molecules for the full PIC; 137, 735, 423, 377 for –eIF3/4B; 1,255, 1,182, 447, 391 for –eIF3/4B/4F, respectively).

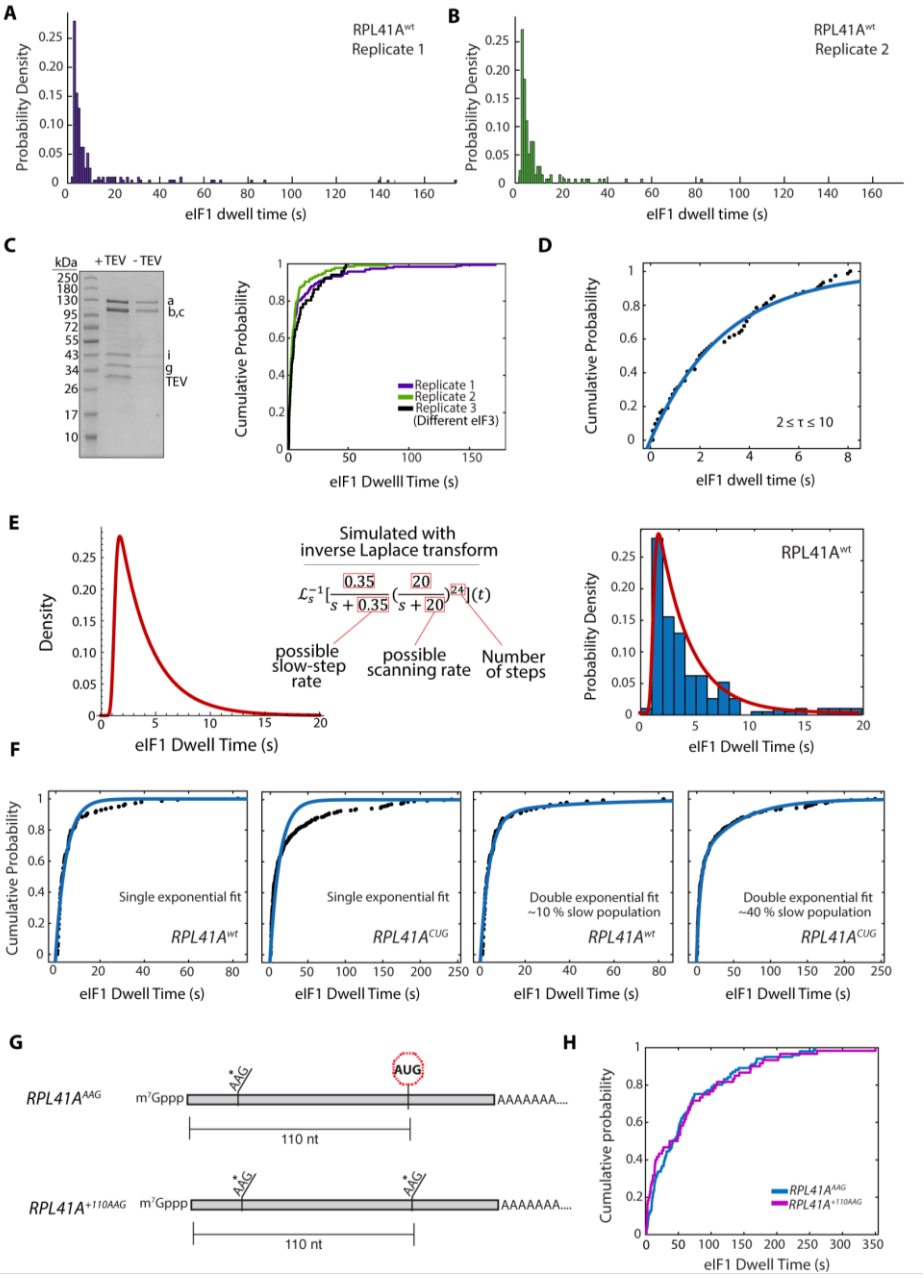

Fig. S3. Evaluation of data reproducibility and kinetic modeling. (A,B) eIF1 dwell-time distribution for the *RPL41A* mRNA in two replicates (n = 193 molecules for the first replicate and n = 136 molecules for the second replicate). **(C)** Comparison of eIF1 dwell-times between eIF3 preparations, with SDS-PAGE verification for removal of residual TEV protease in a second preparation. **(D)** Exponential fit to dwell-time data extracted from the 2 – 10 s time domain of the *RPL41A*^{wt} distribution. **(E)** eIF1 dwell time distribution simulation with inverse Laplace transform for *RPL41A*^{wt}. **(F)** eIF1 dwell- time cumulative distribution functions for scanning on *RPL41A*^{wt} and *RPL41A*^{CUG} fitted to a single and double exponential fit. There is approximately 10 % slow population for *RPL41A*^{wt} and approximately 40 % slow population for *RPL41A*^{CUG}. **(G)** Schematic of *RPL41A*^{AAG} and *RPL41A*$^{+25,+110AAG}$ RNAs. (**H**) eIF1 dwell-time cumulative distribution functions for *RPL41A*^{AAG} and *RPL41A*$^{+25,+110AAG}$ double mutant.

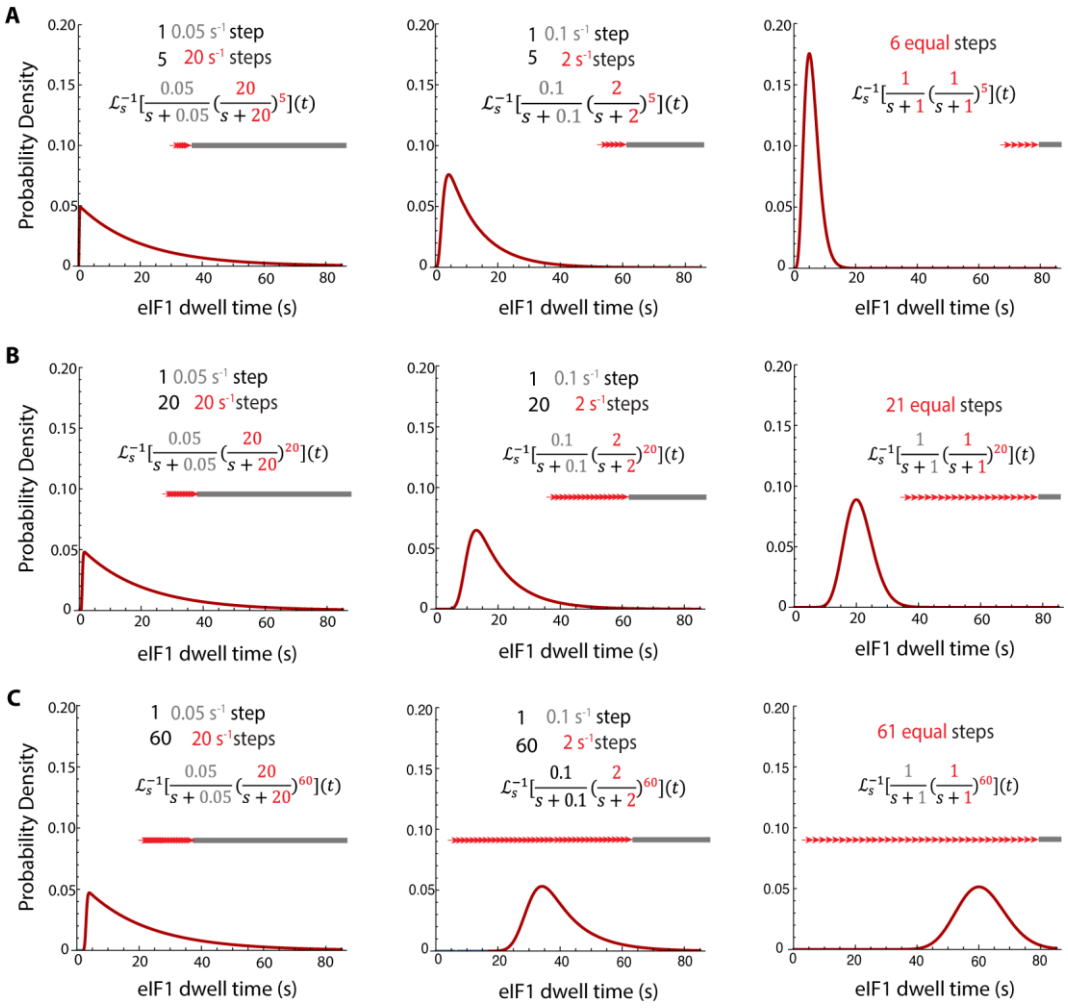

Fig. S4. Simulation of scanning as a multi-step kinetic process. Simulated probability density functions for eIF1 dwell-time distributions under kinetic regimes with varying numbers (top to bottom) and relative timing (left to right) of multiple fast and a single slow step. The model assumes all steps are irreversible. Distributions are generated by inverse Laplace transforms, corresponding to convolution of multiple real-time (exponential) probability density functions. When the single slow step dominates the total passage time, then the distribution is dominated by a single decaying exponential component. However, as the multiple fast steps increasingly dominate the passage time, the distribution becomes more peaked, approaching a normal distribution. **(A)** Models for a pathway of six sequential steps where the multiple fast steps occupy an increasing proportion of the total passage time, moving from left to right. **(B)** Models for a 21-step pathway where an increasing proportion of the total passage time is dominated by multiple fast processes. **(C)** Models for a 61-step pathway where an increasing proportion of the total passage time is dominated by multiple fast processes. The distribution envelopes move further from $t = 0$ as the number of steps increases and becomes narrower with respect to their mean values. The schemes are depicted, for comparison with scanning, with the slow step shown at the end of the sequence. However, equivalent distributions will be obtained regardless of the relative ordering of fast and slow steps.

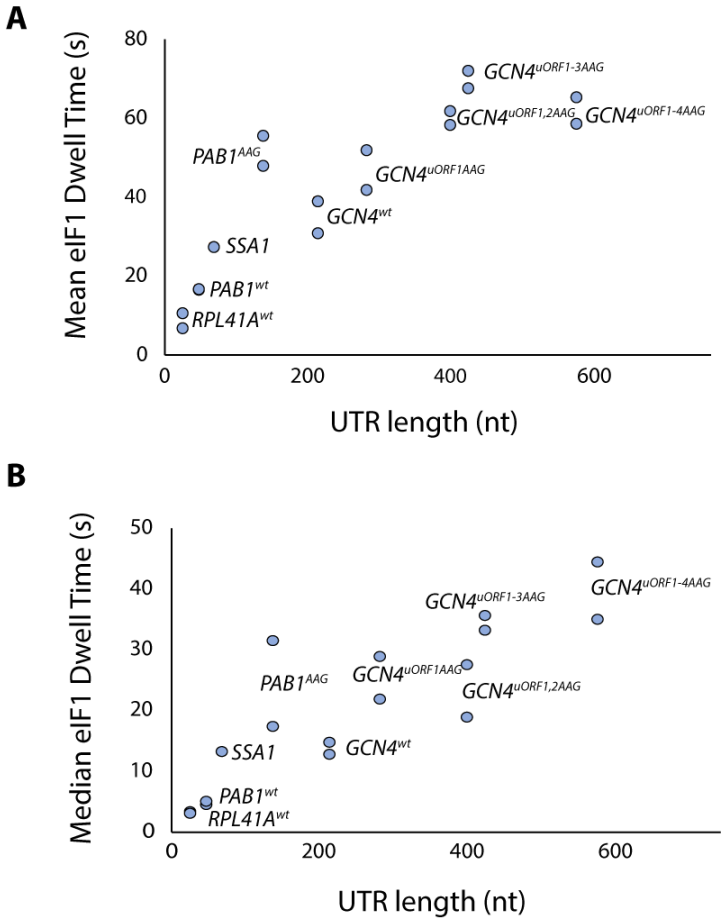

Fig. S5. Global analysis of eIF1 dwell-time dependence on leader length. (A) Scatter plot of mean eIF1 dwell-time values for all RNAs examined in this study. Linear regression indicates a scanning rate of 10.3 nt s^{-1} (95 % confidence intervals: 15.4, 7.7 nt s^{-1}) **(B)** Scatter plot of median eIF1 dwell-time values for all RNAs examined in this study. Linear regression indicates a scanning rate of 16.8 nt s^{-1} (95 % confidence intervals: 24.6, 12.7 nt s^{-1}). For both plots, data from technical replicate experiments are included as separate points.

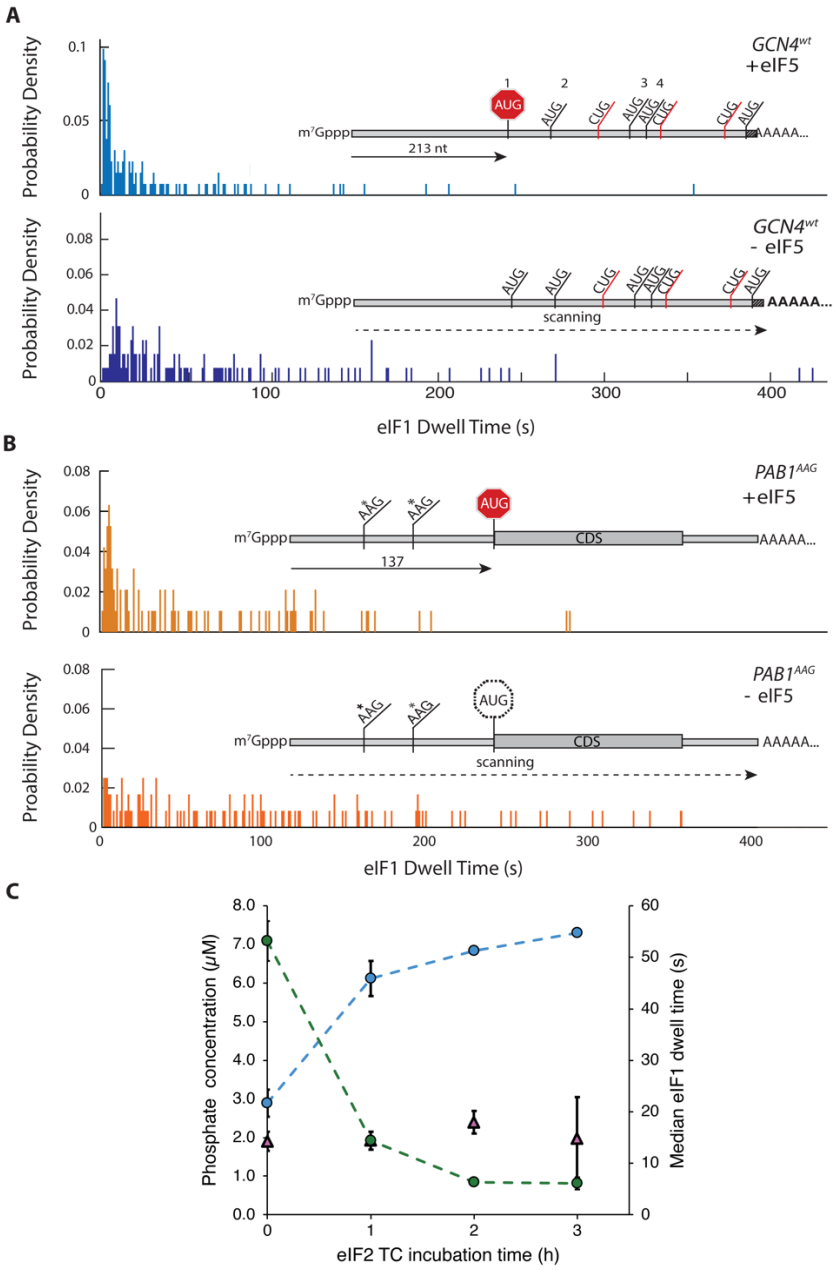

Fig. S6. Effects of eIF5 omission on scanning dynamics. (A) eIF1 dwell-time distribution for the *GCN4*^{wt} mRNA in the presence and absence of eIF5. (n = 273 molecules for full PIC condition and n = 129 molecules for –eIF5 condition). **(B)** eIF1 dwell-time distribution for the *PAB*^{AAG} mRNA with and without eIF5. (n = 95 molecules for the full PIC condition and n = 122 molecules for the –eIF5 condition). **(C)** Effects of eIF2•GDPNP•tRNA$_i^{Met}$ ternary complex pre-incubation on median eIF1 dwell time for scanning on the *RPL41A* mRNA (green dots; y-axis to right). Phosphate concentrations in the incubated ternary-complex sample (blue dots; y-axis to left) and for GDPNP incubated without other ternary-complex components (purple triangles). Error bars for the dwell times represent the standard error from two independent measurements. Error bars for the concentration measurements represent the standard error from three independent measurements.

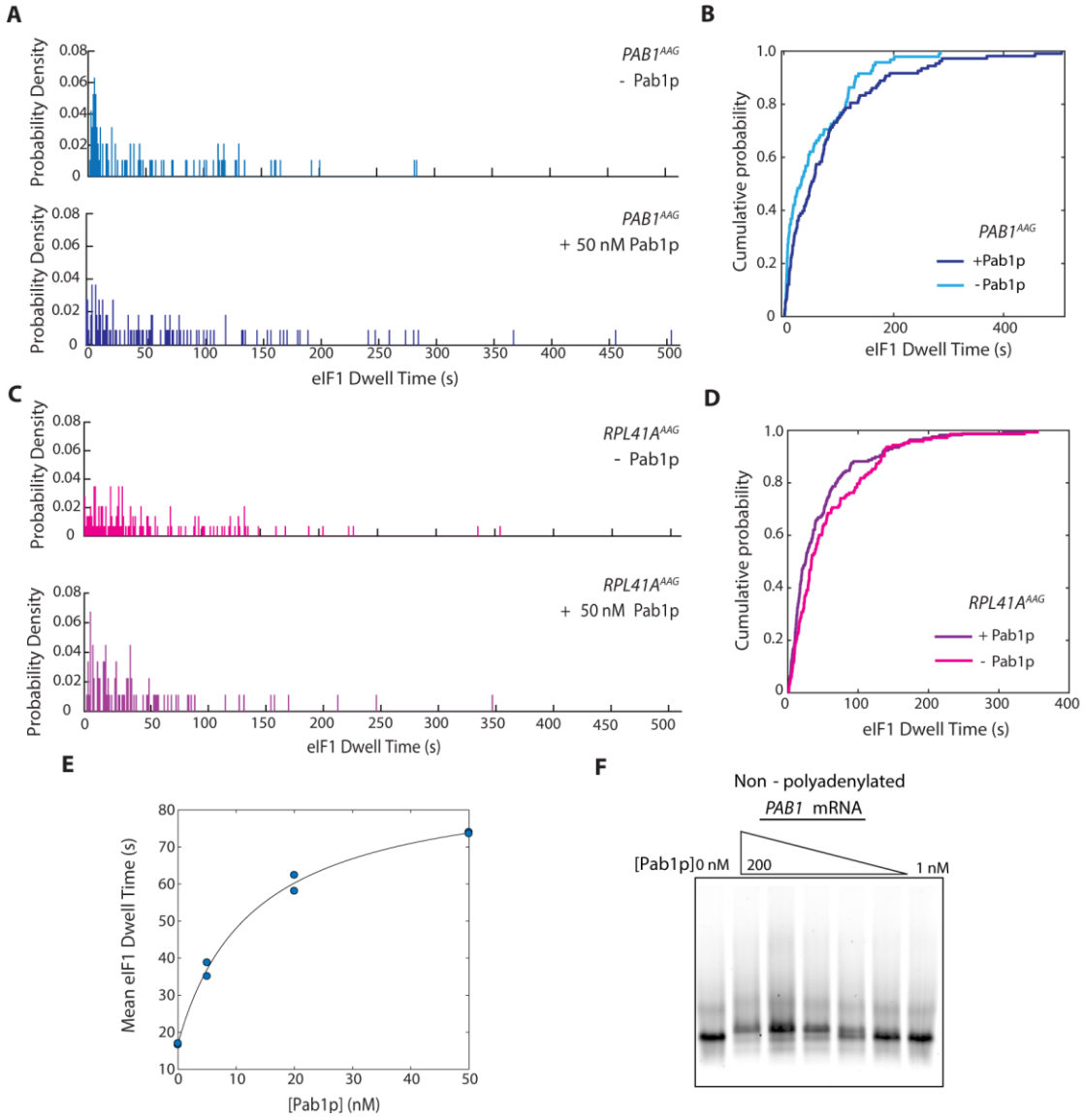

Fig. S7. Effects of Pab1p on scanning dynamics for *PAB1*^{AAG} and *RPL41A*^{wt} mRNAs (A) eIF1 dwell-time distribution for the *PAB*^{AAG} mRNA with and without Pab1p (50 nM). (n = 95 molecules in the absence Pab1p (-Pab1p); n = 108 molecules in the presence of Pab1p (+ 50 nM Pab1p)). **(B)** eIF1 dwell-time cumulative distribution for *PAB*^{AAG} with and without Pab1p (50 nM) **(C)** eIF1 dwell-time distribution for the *RPL41A*^{AAG} mRNA with and without Pab1p (50 nM). (n = 143 molecules in the absence Pab1p (-Pab1p); and n = 169 molecules in the presence of Pab1p (+ 50 nM Pab1p)). **(D)** eIF1 dwell-time cumulative distribution functions for scanning on *RPL41A*^{AAG} with and without Pab1p. **(E)** Hill-Langmuir plot for dependence of mean eIF1 dwell times on the *PAB1* mRNA on the concentration of Pab1p (n_H = 0.98; 95 % confidence intervals: 0.46, 1.51). Replicate data points at 0 nM and 50 nM Pab1p overlap. **(F)** Native electrophoretic mobility shift assay for non-polyadenylated *PAB1* mRNA binding, with varying concentrations of Pab1p (200 to 1 nM) respectively.

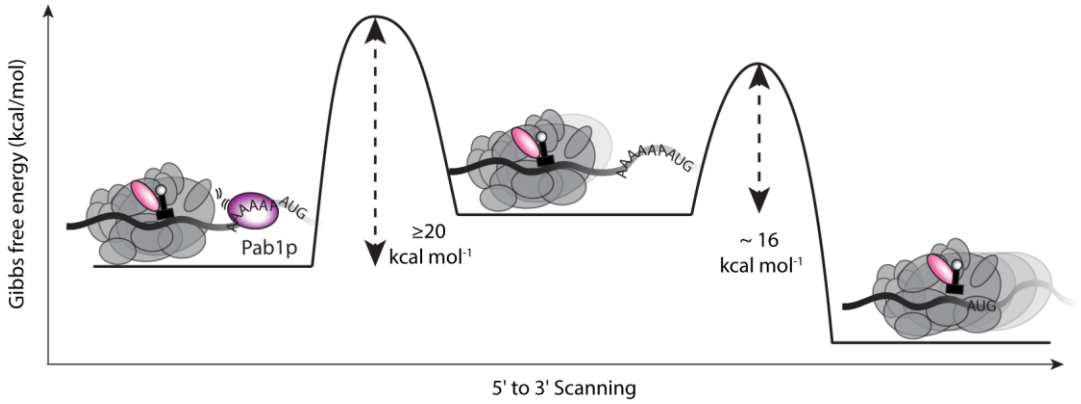

Fig. S8. Mechanistic model for *trans*-regulation of *PAB1* scanning by Pab1p. A steric block to scanning is established by reversible Pab1p binding to the *PAB1* mRNA leader. The proportion of blocked leaders in a population of *PAB1* mRNAs rises saturably with Pab1p concentration. When the PIC arrives at the blockage, it is obliged to wait for Pab1p dissociation before it may resume normal scanning. The scanning delay time added by Pab1p corresponds to a barrier of ~20 kcal mol^{-1} for Pab1p–*PAB1* dissociation.

RPL41A	**Mean (s)**	**Median (s)**
wt	8.8 ± 1.9	3.3 ± 0.1
CUG	28.9 ± 2.5	9.2 ± 2.0
AAG	59.6 ± 1.8	37.7 ± 4.0
AAG, Kozak	62.5 ± 3.8	34.0 ± 3.6
wt + GDPNP	73.9 ± 5.5	47.7 ± 0.9
GCN4	**Mean (s)**	**Median (s)**
wt	35.1 ± 4.1	13.9 ± 1.0
uORF1 AAG	47.0 ± 5.1	25.5 ± 3.5
uORF1,2 AAG	60.2 ± 1.8	23.3 ± 4.3
uORF1-3 AAG	69.9 ± 2.2	35.8 ± 2.5
uORF1-4 AAG	62.1 ± 3.4	39.8 ± 4.7
uORF1-4 AAG + GDPNP	82.1 ± 1.4	53.4 ± 7.5
PAB1	**Mean (s)**	**Median (s)**
wt	16.8 ± 0.2	4.9 ± 0.3
AAG	51.9 ± 3.9	24.6 ± 7.1
wt + 5 nM Pab1p	37.0 ± 1.9	19.5 ± 0.9
wt + 20 nM Pab1p	60.3 ± 2.2	32.6 ± 0.5
wt + 50 nM Pab1p	73.8 ± 0.2	41.2 ± 4.4

Table S1. Calculated means and medians of eIF1 dwell time distribution on *RPL41A*, *GCN4*, and *PAB1* mRNAs under various conditions and modifications.

Data S1. (separate file)
Mean and median eIF1 dwell-time values.